

Jamming Mitigation Based on Improved GNSS/UWB Tightly-Coupled Integration

*Original*

Jamming Mitigation Based on Improved GNSS/UWB Tightly-Coupled Integration / Cao, Z., Mehr, I.E., Liu, J., Guo, Y., DAVIS, F., Jiang, W., Cai, B.. - ELETTRONICO. - (2024), pp. 3665-3678. (The 37th International Technical Meeting of the Satellite Division of The Institute of Navigation (ION GNSS+ 2024) Baltimore (Maryland) September 16 - 20, 2024) [10.33012/2024.19905].

*Availability:*

This version is available at: 11583/2993525 since: 2024-10-18T11:05:46Z

*Publisher:*

Institute of Navigation (ION)

*Published*

DOI:10.33012/2024.19905

*Terms of use:*

This article is made available under terms and conditions as specified in the corresponding bibliographic description in the repository








*Publisher copyright*

GENERICO -- per es. Nature : semplice rinvio dal preprint/submitted, o postprint/AAM [ex default]

The original publication is available at <https://doi.org/10.33012/2024.19905> / <http://dx.doi.org/10.33012/2024.19905>.

(Article begins on next page)

# Jamming Mitigation based on Improved GNSS/UWB Tightly-coupled Integration

Zhuojian Cao <sup>12</sup> , Iman Ebrahimi Mehr <sup>2</sup> , Jiang Liu <sup>13</sup> , Yihan Guo <sup>2</sup> , Fabio Dovis <sup>2</sup> , Wei Jiang <sup>13</sup> , Bai-gen Cai <sup>13</sup> 

<sup>1</sup> School of Automation and Intelligence, Beijing Jiaotong University, Beijing 100044, China

<sup>2</sup> Politecnico di Torino, Department of Electronics and Telecommunications, Turin, Italy

<sup>3</sup> Frontiers Science Center for Smart High-speed Railway System, Beijing Jiaotong University, Beijing 100044, China;

## BIOGRAPHY

**Zhuojian Cao** received a B.S. degree from Nanjing University of Science and Technology in 2018 and an M.S. degree from Beijing Jiaotong University in 2021. She is currently a Ph.D. student in the School of Automation and Intelligence at Beijing Jiaotong University. Her interest is GNSS application in railway, GNSS anti-jamming, and multi-sensor information fusion.

**Iman Ebrahimi Mehr** received the B.Sc. in electronic engineering from Azad University, Tehran, Iran, and his M.Sc. Degree in ICT for smart society from Politecnico di Torino, Turin, Italy, in 2012 and 2021, respectively. He is currently working on his Ph.D. in the Navigation Signal Analysis and Simulation Group, Department of Electronics and Telecommunications, Politecnico di Torino, Torino, Italy. His research interests include Global Navigation Satellite Systems (GNSS) and artificial intelligence applied to positioning, navigation and timing as well as to interference detection and mitigation.

**Jiang Liu** received his B.S. degree and Ph.D. degree in Intelligent Transportation Engineering from Beijing Jiaotong University in 2007 and 2011, respectively. He served as a postdoctoral researcher at the School of Transportation Science and Engineering at Beihang University from 2011 to 2013. He is currently a Professor at the School of Automation and Intelligence, Beijing Jiaotong University. His research interests include satellite-based positioning, intelligent transportation systems, nonlinear filtering and estimation, multi-sensor information fusion, and geographic information systems.

**Yihan Guo** received the B.Sc. degree from Northwestern Polytechnical University, China, in 2016, and the M.Sc. degree from Shanghai Jiaotong University, China, in 2019. He is a Ph.D. student at the Department of Electronics and Telecommunications (DET) of Politecnico di Torino, Turin, Italy, and member of the Navigation Signal Analysis and Simulation - NavSAS - group. His current research interests include integrated navigation systems and the techniques for detecting and mitigating GNSS multipath/NLoS interference.

**Fabio Dovis** received the M.Sc. and Ph.D. degrees from the Politecnico di Torino, Turin, Italy, in 1996 and 2000, respectively. In 2004, he joined the Department of Electronics and Telecommunications, Politecnico di Torino as an Assistant Professor where he has been a full professor since 2021. He coordinates the Navigation Signal Analysis and Simulation Research Group. His research interests include design of GPS and Galileo receivers and advanced signal processing for interference and multipath detection and mitigation, and also ionospheric monitoring. Dr. Dovis is a Member of the IEEE Aerospace and Electronics Systems Society Navigation Systems Panel.

**Wei Jiang** received her Ph.D. degree at the School of Civil and Environmental Engineering, University of New South Wales, Australia. She is a Professor at the School of Automation and Intelligence, Beijing Jiaotong University. Her current research interest is multi-sensor integration and in particular the implementation of new navigation and data fusion algorithms.

**Baigen Cai** received the B.S., M.Sc., and Ph.D. degrees in Traffic Information Engineering and control from Beijing Jiaotong University in 1987, 1990, and 2010, respectively. Since 1990, he has been a Faculty Member with the School of Electronic and Information Engineering, Beijing Jiaotong University. He was a Visiting Scholar with the Ohio State University from 1998 to 1999. He is currently a Professor and the Dean of the School of Automation and Intelligence, Beijing Jiaotong University. His research interests include intelligent transportation systems, GNSS navigation, multi-sensor data fusion, intelligent traffic control, and system modeling & Simulation. Prof. Cai is the project leader for several national and international co-operation research and development research funding. He is also a member of the Chinese Association of Automation and the Deputy Secretary General of the Committee of Experts on the Chinese Urban Rail Transit Association.

## ABSTRACT

Global Navigation Satellite System (GNSS) has been recognized as a crucial information technology for Location-Based Services (LBS) in various fields. However, GNSS is inherently vulnerable to intentional or unintentional Radio Frequency Interference (RFI). Therefore, safety concerns of LBS using GNSS as the main positioning method, especially when suffering from RFI, should be a primary focus. The RFI may severely degrade the performance of GNSS, or even cause the failure of the

receiver's ability to extract measurements. It is of great significance to mitigate the impacts of interference for the safety-critical applications. This work aims at exploiting Ultra-Wide Band (UWB) as aiding information from the integration stage to improve the performance when GNSS suffering from interference. The ranging measurement from UWB anchors can serve as the aiding information to provide positioning information. Due to its operation in the higher frequency band up to several GHz, which is entirely separate from the GNSS frequency bands, thereby ensuring it is immune from GNSS interference. This research develops an improved positioning solution based on the Tightly-coupling (TC) of GNSS and UWB. Based on the field UWB data and a GNSS jamming experimental platform, a half-simulated experimental platform for GNSS and UWB integration under GNSS jamming conditions is established. Test Results under the chirp-jamming scenarios are evaluated to demonstrate the necessity and superiority of the proposed solution.

## I. INTRODUCTION

Global Navigation Satellite System (GNSS) has been recognized as a crucial information technology for Location-based Services (LBS) in various fields, ranging from personal smart devices, Internet of Things (IoT), Intelligent Transportation Systems (ITS), emergency rescue services to precision agriculture and so on. Consequently, the security and reliability of GNSS are highly dependant on the operation of positioning services. However, GNSS signals are vulnerable to RFI, because the received signal power at the ground is extremely low after a long-distance transmission, falling around -130dBm. Furthermore, the public accessibility of its signal structure also exposes GNSS to targeted signal attacks. Jamming, a form of intentional RFI signal generated by jammer devices, aims at disrupt normal operation of GNSS-based services by deliberately transmitting powerful signals in GNSS bands Borio et al. (2016) Zhong et al. (2024). Due to its simplicity and the availability of devices that can execute it, jamming is highlighted as a more common and easily implemented attack on GNSS systems. The realizable low-cost GNSS jamming devices (e.g., personal privacy devices Borio et al. (2016)) are posing a serious threat to GNSS and augmenting the likelihood of degradation in the signal processing procedure of GNSS receivers. They cause difficulty in accurate Position, velocity and timing (PVT) estimation or even denials of GNSS services. To combat these targeted threats, the adoption of anti-jamming technologies and the development of GNSS's ability to safeguard against RFI are crucial for improving the resilience of GNSS-based service.

Resilience for GNSS applications is defined as the system's ability to prepare for, adapt to and recover from changing conditions, including deliberate attacks, unintentional accidents, or nature disturbances House (2013). Specifically, GNSS resilience involves the system's rapid recovery capabilities in response to threats such as jamming or spoofing. Numerous strategies have been developed to enhance defenses against jamming. State-of-the-art mitigation techniques for jamming are organized based on a generalized architectural model of GNSS receivers. This model typically divides the operational workflow into four functional stages: the front-end, pre-correction, post-correlation, and navigation processing stages. The front-end, technological enhancements focus on improving signal resilience at the hardware level. Advanced antenna arrays Yinusa et al. (2018) Zhang et al. (2019) help in mitigating against jamming signals in the early stage. Numerous antennas are put together to form so called antenna arrays. This approach leverages an additional mathematical dimension, enhancing the system capability. However, it also increases the complexity and cost of the system Medina et al. (2019). Moving to the pre-correction stage, methods based on raw GNSS signals exploit the unique properties of different jamming types in domains such as time, frequency or time-frequency. To mitigate the effects of jamming signals, detecting the interference, estimating the waveform and deleting it from the signals are conducted Abd El Rahman et al. (2021). A typical technique is adaptive notch filtering, which identifies the center frequency of the jamming signal to reconstruct its waveform and remove it from the raw Intermediate Frequency (IF) signal Abbasi et al. (2020). However, these methods necessitate considerable computational resources in processing the high-frequency IF signal generated after analog-to-digital conversion. Precise model matching of the jamming signal is critical, otherwise it may lead to mitigation failures. In addition, implementing the aforementioned techniques unavoidably involves structural modifications to the internal design and configuration of the GNSS receiver.

Another way to mitigate the effects of jamming signals on the positioning solution is to integrate it with other sensing sources. The inertial-aiding-based strategy at the information fusion stage provides a different way. Inertial units are not susceptible to radio interference, which makes it possible to mitigate the effects of jamming signals Cao et al. (2022). The mitigation of jamming does not guarantee reliable information when GNSS receiver is completely blinded due to jamming. In this research, we use the Ultra-wide Band (UWB) technique to mitigate the effects of jamming attacks, in the information fusion stage. The utilization of UWB technique releases the requirement for structure modification to the inherent GNSS receiver. Typically, the navigation solution for a GNSS/UWB integration is estimated using the Recursive Bayesian Estimation framework, where the Kalman Filter (KF) is the most commonly employed method Singh (2020). Compared to the most popular Extended Kalman Filter (EKF), the Cubature Kalman Filter (CKF) Arasaratnam and Haykin (2009) offers advantages in positioning estimation. CKF employs a higher-degree cubature rule to compute the Gaussian weighted integrals over the probability density functions. This method provides better approximation accuracy for nonlinear state and measurement models than the first-order linearization used by the common EKF. Given above considerations, this research propose an improved jamming mitigation solution in the measurement stage of the processing chain. By leveraging UWB-aided measurements, a GNSS/UWB Tightly-Coupled (TC) integration based on CKF is used to mitigate the negative effects of jamming signals on the positioning solution.

The main contributions of this work can be summarized as follows:

- Unlike conventional methods that predominantly handle jamming at either the pre-correction or post-correlation stages, This study proposes a novel approach to interference mitigation by exploring the integration of UWB and GNSS within the measurement stage and develops a CKF-based TC integration solution for jamming mitigation.
- This research develops a comprehensive GNSS jamming test platform that utilizes open-sky satellite signals, enabling the controlled simulation of various jamming scenarios. Coupled with real-collected UWB ranging measurements, the tests are conducted to evaluate and verify the interference mitigation capabilities of the proposed solution.

The remainder of this paper is organized as follows. Section II provides the background of the proposed solution, including analyses of GNSS and interference, as well as UWB. The detailed proposed solution is described in Section III. Section IV presents the experimental setup and results. Section V discusses the conclusion and future work.

## II. BACKGROUND

### 1. GNSS and interference analysis

Direct Sequence Spread Spectrum (DSSS) technology is applied to GNSS signals, which, in many cases, provides the system with a sufficient degree of interference blocker rejection. However, when the interference power is too high, especially considering the inherently low power of GNSS signals, the signal processing capabilities of GNSS receivers may not be sufficient to achieve a satisfied system performance level.

The received signal of  $i$ -th satellite at the antenna is given as follows for a single frequency :

$$s^{(i)}(t) = \sqrt{P_c} x^{(i)}(t - \tau^{(i)}) D^{(i)}(t - \tau^{(i)}) \exp\left(j\left(2\pi\left(f_1 + f_d^{(i)}\right)(t - \tau^{(i)}) + \theta^{(i)}\right)\right) \quad (1)$$

where  $P_c$  denotes the received power of the  $i$ -th satellite's signal;  $x^{(i)}(t)$  represents the spreading code;  $D^{(i)}(t)$  is the navigation data bit;  $\theta^{(i)}$  is the initial phase;  $\tau^{(i)}$  is the code delay;  $f_d^{(i)}$  is the Doppler shift and the carrier phase is synchronized with the L1 frequency carrier  $f_1$ . The overall signal received by a GNSS receiver at epoch  $t$  is composed of the combined signals from all in-view satellites  $\sum_i s^{(i)}(t)$ , along with the background noise  $n(t)$  over the propagation channel and a possible jamming signal  $j(t)$ . Therefore, the overall received signal  $r(t)$  can be written as:

$$r(t) = \sum_i s^{(i)}(t) + n(t) + j(t) \quad (2)$$

Several researches, referenced as Borio et al. (2016), Morales Ferre et al. (2019), Kraus et al. (2011), have explored the problem of describing the jamming signal  $j(t)$ . These signals are predominantly used by attackers and are typically designed to broadcast frequency-modulated signals with a periodic behavior. The center frequency of the jamming signal scans a certain frequency band according to a periodic pattern, that, in some cases, corresponds to a linear function, also called Chirp signal. This chirp signal can be modelled as:

$$j(t) = \sqrt{P_c} \exp\left(j\left(2\pi f_c t + \pi \frac{f_{\max} - f_{\min}}{T} t^2 + \theta_c\right)\right) \quad (3)$$

where  $f_c$  is the initial sweep frequency,  $f_{\min}$  and  $f_{\max}$  are the minimum and maximum frequency of chirp signal,  $T$  represents sweep period and  $\theta_c$  is the initial phase. After preamplifier, down convertor, and A/D convertor to the received signal, the digital correlation process of the GNSS receiver spreads the narrow-band jamming signal into a wide-band signal, while despreading the expected signal into a narrowband (data modulation) signal. This is a significant signal bandwidth reduction of expected signal and interference bandwidth expansion. Consequently, the interference is generally equivalent to white noise, which means the spectra of either the interference or the desired signal is well approximated by a straight line over a bandwidth that is the reciprocal of the integration time used in the correction Kaplan and Hegarty (2017). The quality of a received GNSS signal is commonly described in terms of its carrier-to-noise-density ratio ( $C/N_0$ ). For analysis, it is possible to define an equivalent carrier-to-noise-density that, when applied to the system, produces the same output as the combination of the actual white noise and interference. The effective  $(C/N_0)_{\text{eff}}$  expressed in units of dB-Hz to describe the signal quality in the presence

of interference can be formulated as Kaplan and Hegarty (2017):

$$(C/N_0)_{\text{eff, dB}} \triangleq 10 \log_{10} (C/N_0)_{\text{eff}}$$

$$= -10 \log_{10} \left[ 10^{-\frac{(C/N_0)_{\text{dB}}}{10}} + \frac{10^{\frac{(C_j/C)_{\text{dB}}}{10}}}{Q \cdot f_c} \right] \quad (4)$$

where  $f_c$  is the rate of pseudo-code, the rate of Global Positioning System (GPS)  $C/A$  code is 1.023MHz;  $C/N_0$  is the carrier-to-noise-density ratio;  $C_j/C$  is the jamming-to-received-signal power ratio inside the receiver,  $Q$  is a dimensionless jamming resistance quality factor to be determined for various types of jammers and signal modulations. A higher jamming resistance quality factor  $Q$ , results in increased jamming effectiveness. The coefficient  $1/(Q \cdot f_c)$  is the normalized power ratio of the jammed GNSS within the jamming band to the normal GNSS in whole band Ding et al. (2023). Thermal noise covers the whole GNSS spectrum, while jamming signals interfere GNSS spectrum at a specific jamming band. In this paper, we use Jamming-to-Signal Ratio (JSR) in decibels at the antenna input to quantify the relationship between GNSS signal power and jamming power. The effective  $(C/N_0)_{\text{eff}}$  decreases as JSR increasing under fixed  $C/N_0$ , until resulting in the loss of lock of GNSS receiver. The impact of increasing  $(C/N_0)_{\text{eff}}$  on the code phase estimation may result in greater variance, as well as measurement bias of the target receiver, thus leading to a degraded performance in accuracy of the position estimation.

## 2. UWB analysis

By transmitting extremely short pulses of time (i.e., nanoseconds or less) and occupying a large bandwidth over 500MHz, UWB technology achieves precise time-of-flight ranging measurements. To facilitate the coordination of existing spectral allocation schemes with UWB signals, the First Report and Order from Federal Communications Commission (FCC) Commission et al. (2002) allows unlicensed use of spectrum for UWB technology mainly between 3.1GHz and 10.6GHz at extremely low power (maximum of -41.3dBm/MHz, which is only higher than the noise floor) Aiello and Rogerson (2003). DW1000 DecaWave (2015), a typical UWB chip used in our research, offers Two-way Time-of-flight (TW-TOF)ranging measurements, occupying the frequency band with a center frequency of 3.9936GHz. It should be noted that the GNSS spectrum, ranging from 1 to 2GHz for all constellations, operates independently of the UWB spectrum. There is no frequency overlap of these systems, ensuring that UWB devices and GNSS systems can operate concurrently without causing interference to each other. Furthermore, jamming signals which target to suppress GNSS signals, generally work across the GNSS frequency band. The spectrum allocation of these associated systems is depicted in Fig. 1.

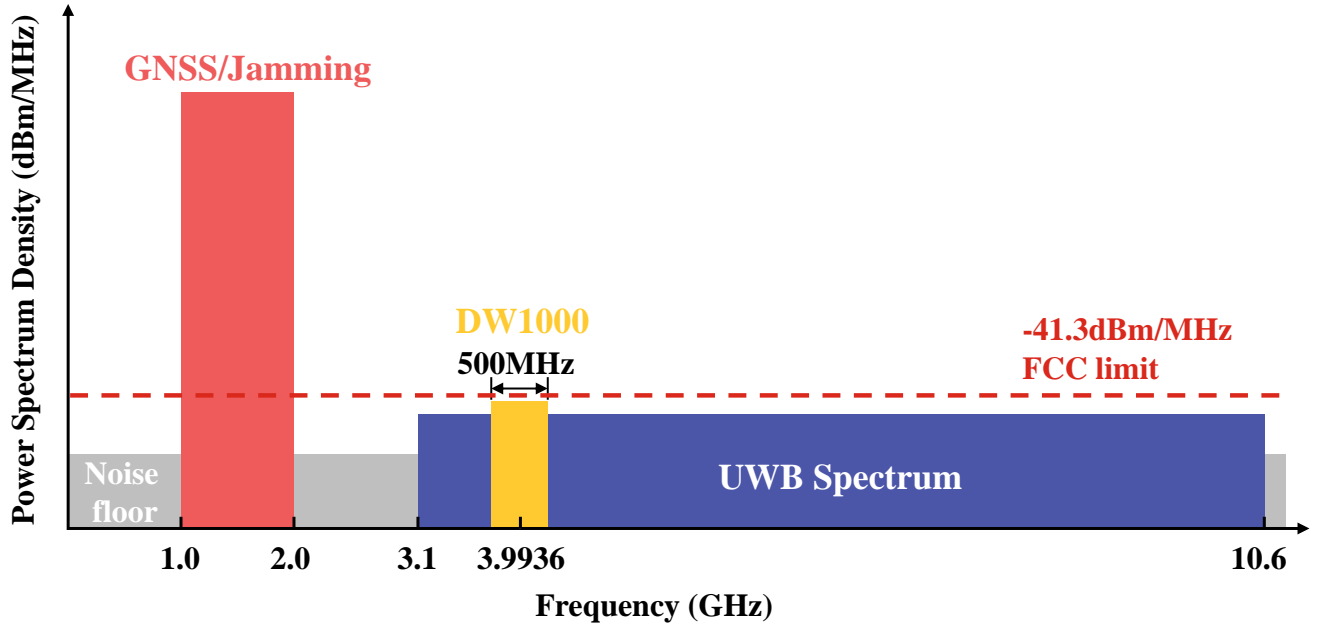


Figure 1: Spectrum allocation and Power Spectrum Density for GNSS, UWB, and DW1000.

This frequency isolation makes UWB immune to interference that commonly affects GNSS. As a result, in environments

where GNSS signals may be interfered by targeted attacks, UWB can serve as an alternative or complementary technology, enhancing the reliability and availability of positioning in critical applications. On the other hand, the compatibility in distance measurement methodologies between UWB and GNSS makes them conducive to integration due to their similar principles of ranging estimation.

### III. PROPOSED SOLUTION

In this research, UWB ranging measurements are employed to protect the distraction on GNSS from interference signals in the measurement and fusion domain, releasing the requirement for structural modifications inside the GNSS receiver. This enables the GNSS-based LBS systems to use a non-resilient GNSS chipset (a chipset that does not make any efforts to enhance resilience) and integrate it with UWB measurements in a compatibility way that will eventually prevent the positioning solution from degradation or even failure caused by GNSS jamming signals.

#### 1. System Models

For GNSS, it enables two basic types of measurements, including pseudorange and Doppler shift. The pseudorange measures the satellite in view (SV)-receiver distance, except for the asynchronicity of the two clocks and some other delays. Given a SV  $i$  at epoch  $k$ , the pseudorange measurement model is formulated as (5)

$$\rho_{G,k}^{(i)} = D_{\text{Ecd}} \left( \mathbf{p}_{G,k}^{(i)}, \mathbf{p}_{r,k} \right) + T_k^{(i)} + I_k^{(i)} + c \left( dt_{r,k} - dt_k^{(i)} \right) + \epsilon_{G,k}^{(i)} \quad (5)$$

where:

- $\mathbf{p}_{G,k}^{(i)}$  and  $\mathbf{p}_{r,k}$  are the position vector of SV  $i$  and the receiver at epoch  $k$ , respectively. Both vectors are referred to an Earth-centered, Earth-fixed (ECEF) coordinate frame;
- $D_{\text{Ecd}}(\mathbf{u}, \mathbf{v})$  represents the Euclidean norm of  $\mathbf{u} - \mathbf{v}$ , which means  $D_{\text{Ecd}} \left( \mathbf{p}_{G,k}^{(i)}, \mathbf{p}_{r,k} \right)$  is the physical distance between the SV  $i$  and the GNSS receiver at epoch  $k$ ;
- $T_k^{(i)}$  and  $I_k^{(i)}$  are the tropospheric delay and ionospheric delay of SV  $i$ , respectively;
- $dt_{r,k}$  and  $dt_k^{(i)}$  are the receiver clock bias and the  $i$ -th SV clock bias at epoch  $k$ , respectively;
- $\epsilon_{G,k}^{(i)}$  accounts for all unmodeled errors including receiver noise and interference effects, etc.

Caused by the relative motion of the receiver and satellite, the observed frequency of a signal from a satellite differs from its nominal frequency, which is known as Doppler shift. The pseudorange rate can be derived from the Doppler shift following (6).

$$\underbrace{\dot{\rho}_{G,k}^{(i)}}_{\lambda \cdot d_{G,k}^{(i)}} = \left[ \mathbf{v}_{G,k}^{(i)} - \mathbf{v}_{r,k} \right]^T \cdot \mathbf{e}_k^{(i)} + c \left( \dot{dt}_{r,k} - \dot{dt}_k^{(i)} \right) + \dot{\epsilon}_{G,k}^{(i)} \quad (6)$$

where:

- $\lambda$  is the carrier wave length;
- $d_{G,k}^{(i)}$  is the Doppler shift measurement of GNSS receiver;
- $\mathbf{v}_{G,k}^{(i)}$  and  $\mathbf{v}_{r,k}$  are the velocity vectors of the GNSS receiver and the  $i$ -th SV at epoch  $k$ , respectively. Note that they are both in ECEF coordinate frame.
- $\mathbf{e}_k^{(i)}$  is the line-of-sight vector from the receiver to the  $i$ -th SV position at epoch  $k$  in ECEF coordinates;
- $\dot{dt}_{r,k}$  and  $\dot{dt}_k^{(i)}$  are the clock drift of the receiver and the  $i$ -th SV, respectively.
- $\dot{\epsilon}_{G,k}^{(i)}$  accounts for all unmodeled errors.

Furthermore, the UWB system calculates the distance between an anchor and a tag using the TW-TOF ranging method. This technique is employed by at least two commercial devices of UWB ranging equipment. By measuring the time it takes for an impulse signal to travel from a transmitter (typically a fixed anchor at a known position) to a receiver (a moving tag designed as

the target), it allows us to get the precise distance between the anchor and the tag. The UWB ranging model at epoch  $k$  can be written as:

$$\rho_{U,k}^{(j)} = D_{\text{Ecd}} \left( \mathbf{p}_{U,k}^{(j)}, \mathbf{p}_{r,k}^U \right) + \epsilon_{U,k}^{(j)} \quad (7)$$

where:

- $\rho_{U,k}^{(j)}$  is the measured distance from the anchor  $j$  to the tag at epoch  $k$ ;
- $\mathbf{p}_{U,k}^{(j)}$  and  $\mathbf{p}_{r,k}^U$  are the the position vector of  $j$ -th anchor and the tag at epoch  $k$ , respectively;
- $\epsilon_{U,k}^{(j)}$  accounts for all unmodeled errors, modeled as Gaussian white noise.

Due to the extremely short and high-frequency pulses transmitted by UWB systems, UWB signals achieve exceptionally fine time resolution. The noise item  $\epsilon_{U,k}^{(j)}$  in the equation is modeled as  $\epsilon_{U,k}^{(j)} \sim \mathcal{N}(0, \sigma_U^2)$  where  $\sigma_U$  is typically considered to be in centimeter level.

## 2. CKF-based Tightly-coupled Integration

In this subsection, a TC positioning system that enhances GNSS-based positioning with UWB under interference conditions is presented. The KF is used here to recursively estimate the random states of the dynamic system that minimizes the mean squared prediction error. A constant velocity dynamic model is adopted in this subsection for a static carrier, assuming that the carrier moves at a constant velocity, which is particularly well-suitable for tracking low-dynamic carriers. Given that the experiments were conducted in a static scenario, the constant velocity model is employed here. Nevertheless, it is possible to extend this solution to a dynamic scenario, in which a constant acceleration model would be more appropriate. An 8-dimensional error state vector is defined to describe the required states as shown in (8)

$$\mathbf{x}(t) = [\delta \mathbf{p} \quad \delta \mathbf{v} \quad \delta dt_r \quad \delta \dot{dt}_r]^T \quad (8)$$

where  $\mathbf{x}(t)$  is the continuous state vector;  $\delta \mathbf{p}$  is the position error in three dimensions;  $\delta \mathbf{v}$  is the velocity error;  $\delta dt_r$  and  $\delta \dot{dt}_r$  are the receiver clock bias, and drift, respectively. The state space differential equation is expressed as  $\dot{\mathbf{x}}(t) = \mathbf{F}(t) \mathbf{x}(t) + \boldsymbol{\omega}(t)$ , in which the system dynamic matrix  $\mathbf{F}(t)$  is defined as:

$$\mathbf{F}(t) = \begin{bmatrix} \mathbf{0}_{3 \times 3} & \mathbf{I}_{3 \times 3} & 0 & 0 \\ \mathbf{0}_{3 \times 3} & \mathbf{0}_{3 \times 3} & 0 & 0 \\ \mathbf{0}_{3 \times 3} & \mathbf{0}_{3 \times 3} & 0 & 1 \\ \mathbf{0}_{3 \times 3} & \mathbf{0}_{3 \times 3} & 0 & 0 \end{bmatrix} \quad (9)$$

Equation (9) can be converted into discrete-time state model at epoch  $k$ :  $\mathbf{x}_k = \Phi_k \mathbf{x}_{k-1} + \boldsymbol{\eta}_{k-1}$ , where  $\mathbf{x}_k = \mathbf{x}(t_k)$  by defining the discrete-time interval as  $T_s = t_k - t_{k-1}$ .  $\boldsymbol{\eta}_{k-1}$  is the discrete-time kinematic noise, satisfying  $E(\boldsymbol{\eta}_{k-1} \boldsymbol{\eta}_{k-1}^T) = \mathbf{Q}_{k-1}$ . The discrete-time state transition matrix  $\Phi_k$  is given as (10)

$$\Phi_k = \begin{bmatrix} \mathbf{I}_{3 \times 3} & T_s \mathbf{I}_{3 \times 3} & 0 & 0 \\ \mathbf{0}_{3 \times 3} & \mathbf{I}_{3 \times 3} & 0 & 0 \\ 0 & 0 & 1 & T_s \\ 0 & 0 & 0 & 1 \end{bmatrix} \quad (10)$$

Owing to the linearity of the state space model, a linear time updating procedure can be performed to release the computation burden. Additionally, the Extended Kalman Filter (EKF) is capable of carrying out TC integration by linearizing the measurement model based on the first-order derivative. However, it suffers from substantial approximation errors in highly nonlinear cases. Cubature Kalman Filter utilizes cubature rules to approximate the integrals needed for the posterior mean and covariance estimation rather than linearizing the system, which can lead to an enhanced performance level. The discrete-time measurement model of the filter is given as

$$\mathbf{z}_k = \mathbf{h}_k(\mathbf{x}_k) + \mathbf{v}_k \quad (11)$$

where  $\mathbf{z}_k$  is the observation vector,  $\mathbf{h}_k(\cdot)$  is the nonlinear function which is built based on equations (5) and (6);  $\mathbf{v}_k$  is the measurement noise satisfying  $\mathbf{v}_k \sim \mathcal{N}(\mathbf{v}_k; \mathbf{0}, \mathbf{R}_k)$ . In GNSS dynamic positioning, the differences between the observations

corresponding to estimated states and GNSS measurements are taken as the system observations. The observation vector is defined as

$$\mathbf{z}_{G,k} = \left[ \rho_{G,k}^{(1)} - \dot{\rho}_{0,k}^{(1)} \quad \dots \quad \rho_{G,k}^{(n)} - \dot{\rho}_{0,k}^{(n)} \quad \dot{\rho}_{G,k}^{(1)} - \dot{\rho}_{0,k}^{(1)} \quad \dots \quad \dot{\rho}_{G,k}^{(n)} - \dot{\rho}_{0,k}^{(n)} \right]^T \quad (12)$$

where  $\rho_{G,k}^{(*)}$  and  $\dot{\rho}_{G,k}^{(*)}$  are, the error-eliminated pseudorange and range rate of the  $i$ -th SV;  $\rho_{0,k}^{(*)}$  and  $\dot{\rho}_{0,k}^{(*)}$  are the range and range rate corresponding to a specific estimated state. With the enhancement of UWB ranging measurements, the UWB measurements can be fed into the measurement model as well, aiding positioning results to defend against the degradation resulted by GNSS interference signals and enhancing the resilience. The observation vector related to UWB ranging is given as

$$\mathbf{z}_{U,k} = \left[ \rho_{U,k}^{(1)} - \rho_{0,k}^{(1)} \quad \dots \quad \rho_{U,k}^{(m)} - \rho_{0,k}^{(m)} \right]^T \quad (13)$$

where  $\rho_{U,k}^{(*)}$  is the range measurement from the UWB anchor to the receiver. With the state space model and the measurement space model, the CKF estimation is performed to compensate for the result inferred from the constant velocity model. CKF uses a set of deterministic weighted points to address the non-linear propagation. The propagation rule is described as

$$\int_{\mathbb{R}^n} g(\mathbf{x}) \mathcal{N}(\mathbf{x}; \boldsymbol{\mu}, \boldsymbol{\Sigma}) d\mathbf{x} \approx \sum_{i=1}^N \omega_i g(\boldsymbol{\mu} + \sqrt{\boldsymbol{\Sigma}} \cdot \boldsymbol{\xi}_i) \quad (14)$$

where  $\boldsymbol{\mu} + \sqrt{\boldsymbol{\Sigma}} \cdot \boldsymbol{\xi}_i$  and  $\omega_i$  are cubature points and corresponding weights of Gaussian density  $\mathcal{N}(\mathbf{x}; \boldsymbol{\mu}, \boldsymbol{\Sigma})$ , and they are given by  $\boldsymbol{\xi}_i = \sqrt{m/2} \cdot [1]_i$ ,  $\omega_i = 1/m (i = 1, 2, \dots, m = 2n)$  where  $n$  represents the dimension of  $\mathbf{x}$ ,  $\sqrt{\boldsymbol{\Sigma}}$  is the Cholesky decomposition of  $\boldsymbol{\Sigma}$ . Considering the space model given by (9) and (11), the focus of the estimation problem is to determine the posterior probability density  $p(\mathbf{x}_k | \mathbf{z}_k) \sim \mathcal{N}(\mathbf{x}_k; \hat{\mathbf{x}}_{k|k}, \mathbf{P}_{k|k})$  at epoch  $k$  when given the posterior probability  $p(\mathbf{x}_{k-1} | \mathbf{z}_{k-1}) \sim \mathcal{N}(\mathbf{x}_{k-1}; \hat{\mathbf{x}}_{k-1|k-1}, \mathbf{P}_{k-1|k-1})$  at epoch  $k-1$ . The estimation procedure in the UWB-enhanced positioning solution handled by CKF is given by following steps. Note that the error state is used here.

1. Positioning Status Prediction: Following the constant-velocity dynamic model, the positioning status at epoch  $k$  can be calculated based on the status at epoch  $k-1$ . The positioning status consists of  $Status = \{ \mathbf{p}_k, \mathbf{v}_k, dt_k, \dot{dt}_k \}$ .
2. Time Updating of the State: Initiating the error state  $\hat{\mathbf{x}}_{k-1} = \mathbf{0}$ , and the process noise covariance  $\mathbf{Q}_{k-1}$ . Then predicting the prior density  $p(\mathbf{x}_k | \mathbf{z}_{k-1}) \sim \mathcal{N}(\mathbf{x}_k; \hat{\mathbf{x}}_{k|k-1}, \mathbf{P}_{k|k-1})$ . This procedure can be performed as the standard owing to the linearity of the state space model, given as

$$\hat{\mathbf{x}}_{k|k-1} = \mathbf{F}_{k-1} \hat{\mathbf{x}}_{k-1|k-1} = \mathbf{0} \quad (15)$$

$$\mathbf{P}_{k|k-1} = \mathbf{F}_{k-1} \mathbf{P}_{k-1|k-1} \mathbf{F}_{k-1}^T + \mathbf{Q}_{k-1} \quad (16)$$

3. Measurement Updating: The prior probability density is corrected to the posterior  $p(\mathbf{x}_k | \mathbf{z}_k)$  upon the receipt of new measurements in  $\mathbf{z}_k$ . This correction occurs whenever data is received, regardless of the sensor source. The measurements may originate solely from either GNSS ( $\mathbf{z}_{G,k}$ ) or UWB ( $\mathbf{z}_{U,k}$ ) when these sensors operate asynchronously, or from both sensors concurrently ( $\mathbf{z}_k = [\mathbf{z}_{G,k}, \mathbf{z}_{U,k}]^T$ ) if they function synchronously. In the case of asynchronous data, the filter dynamically adjusts its internal time step ( $T_s$ ). By propagating the cubatures points of  $p(\mathbf{x}_k | \mathbf{z}_{k-1})$  through a nonlinear function  $h_k(\cdot)$ , the measurement likelihood density  $p(\mathbf{z}_k | \mathbf{x}_k) \sim \mathcal{N}(\mathbf{z}_k; \hat{\mathbf{z}}_{k|k-1}, \mathbf{P}_{k|k-1}^{zz})$  can be derived as

$$\boldsymbol{\chi}_{i,k|k-1} = \hat{\mathbf{x}}_{k|k-1} + \sqrt{\mathbf{P}_{k|k-1}} \boldsymbol{\xi}_i \quad (17)$$

$$\mathbf{Z}_{i,k|k-1} = h_k(\boldsymbol{\chi}_{i,k|k-1}) \quad (18)$$

$$\hat{\mathbf{z}}_{k|k-1} = 1/m \sum_{i=1}^m \mathbf{Z}_{i,k|k-1} \quad (19)$$

$$\mathbf{P}_{k|k-1}^{zz} = 1/m \sum_{i=1}^m (\mathbf{z}_{i,k|k-1} - \hat{\mathbf{z}}_{k|k-1}) (\mathbf{z}_{i,k|k-1} - \hat{\mathbf{z}}_{k|k-1})^T + \mathbf{R}_k \quad (20)$$

Then, the conditional Gaussian density of the joint state and the measurement require for the cross-covariance, as follows.

$$\mathbf{P}_{k|k-1}^{xz} = 1/m \sum_{i=1}^m (\boldsymbol{\chi}_{i,k|k-1} - \hat{\boldsymbol{x}}_{k|k-1}) (\mathbf{z}_{i,k|k-1} - \hat{\mathbf{z}}_{k|k-1})^T + \mathbf{R}_k \quad (21)$$

When receiving new measurement, the filter computes the posterior density by

$$\mathbf{K}_k = \mathbf{P}_{k|k-1}^{xz} (\mathbf{P}_{k|k-1}^{zz})^{-1} \quad (22)$$

$$\hat{\boldsymbol{x}}_{k|k} = \hat{\boldsymbol{x}}_{k|k-1} + \mathbf{K}_k (\mathbf{z}_k - \hat{\mathbf{z}}_{k|k-1}) \quad (23)$$

$$\mathbf{P}_{k|k} = \mathbf{P}_{k|k-1} - \mathbf{K}_k \mathbf{P}_{k|k-1}^{zz} \mathbf{K}_k^T \quad (24)$$

4. Positioning Status Correction: The predicted positioning status is corrected based on the estimated error states of epoch  $k$ , which consists of  $\hat{\boldsymbol{x}}_{k|k} = [\delta \mathbf{p}_k, \delta \mathbf{v}_k, \delta dt_{r,k}, \delta dt_{t,k}]$ . By adding the estimated error state  $\hat{\boldsymbol{x}}_{k|k}$  to the predicted positioning status  $Status_{k|k-1}$ , we can get the posterior estimation of the positioning status, given as

$$Status_k = Status_{k|k-1} + \hat{\boldsymbol{x}}_{k|k} \quad (25)$$

The above steps outline the algorithm for UWB-enhanced TC positioning under interference conditions using the Cubature Kalman Filter (CKF). The algorithm iteratively performs positioning status prediction, time updating, measurement updating, and positioning status correction following time stamps.

## IV. EXPERIMENTAL FINDINGS AND ANALYSIS

### 1. Experimental settings

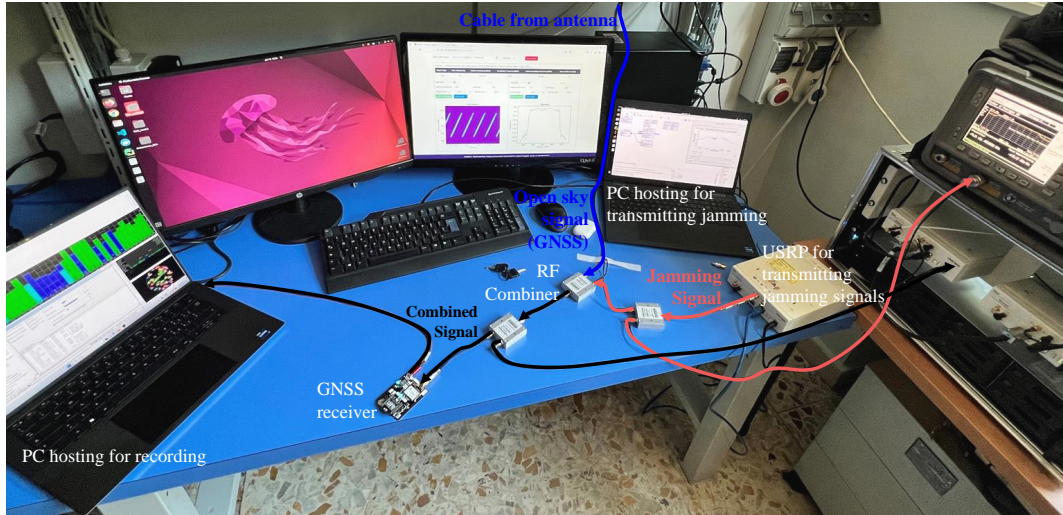


**Figure 2:** The GNSS jamming experimental platform.

A half-simulated experimental platform for GNSS and UWB integration under GNSS jamming conditions is established. Given the experiment involves a static scenario, GNSS and UWB are collected asynchronously. The GNSS signal is received through an open-sky antenna, combined with a jamming signal, and the raw measurements is recorded by the under-test receiver in various jamming power levels. The UWB data is collected asynchronously using three anchors and one tag. We collect three static ranging measurements and simulate the tag at the same location as the GNSS antenna for integration.

Fig. 2 shows the hardware installation of the GNSS jamming experimental platform and its configuration in operation. In the figure, the blue cable represents the open-sky signal from satellites, the pink cable carries the jamming signal, and the black cable carries the combined signal of both. The open-sky radio frequency signal is captured using an antenna installed on

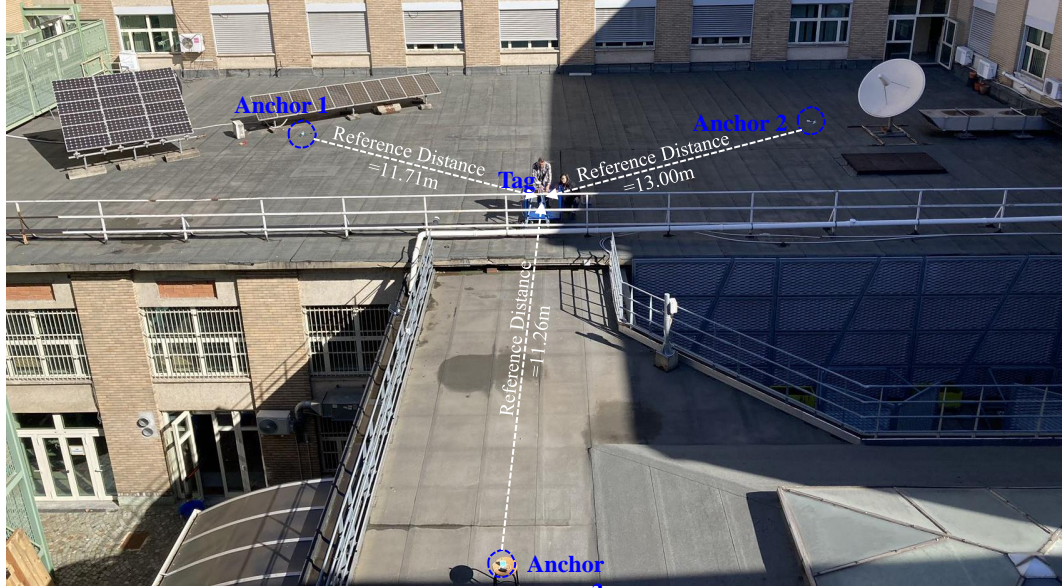


**Figure 3:** The UWB test scenario setting.

the roof at Politecnico di Torino. A Universal Software Radio Peripheral (USRP) N-210 device is used to generate real-time interference signal, specifically a chirp signal in our tests. These two signals from two cables are combined by an RF combiner and transmitted to the GNSS receiver under test (Ublox). A laptop connecting the GNSS receiver runs Ublox Center software to display the positioning status of the receiver. The jamming signal is also transmitted to a spectrum analyzer to visualize the frequency spectrum. Meanwhile, another USRP is connected to the combined signal to collect signal data for analysis.

Additionally, Fig. 3 shows the configuration of the UWB test scenario where three UWB anchors and a tag are set. In this experimental setup, the UWB anchors and the tag are equipped with Decawave's DW1000 chips. The chips are set to occupy 500MHz frequency band centered at 3.9956GHz in the UWB spectrum. The UWB anchors are strategically placed at different positions on a rooftop to form a triangulation area, as depicted in Fig. 3. The UWB tag is statically located on the center among these three anchors. Ranging data in 20Hz from these three anchors are collected, whose reference value are, respectively, 11.71m for Anchor 1, 13.00m for Anchor 2, and 11.26m for Anchor 3. Then, to integrate this UWB scenario into the GNSS platform, the position of the UWB tag is simulated to correspond to the GNSS antenna's location, using the same ECEF coordinates. The relative positions of the three UWB anchors with respect to the tag remain unchanged. In this experimental configuration, the ranging measurements from the three UWB anchors are real data, while the positions of the tag and the anchors are subsequently simulated to match the GNSS platform.

The test is conducted on six different power levels of linear chirp jamming signals, and six sets of GNSS Rinex files under chirp interference are generated. Besides, a jamming-free scenario is also tested for comparison. Then, the measurements from the GPS L1 band are used for analysis and verification. Parameters of GNSS, UWB and interference signals are detailed in Table 1.

## 2. Results and analysis

To visually assess the impact of various jamming powers on the receiver under-test, we analyse the pseudorange residuals using Single-point Positioning (SPP) solution. The pseudorange residuals from six satellites are shown in Fig. 4. The highest jamming power that we tested is -65dBm (30dB of JSR). Notably, there is no residual data of the -65dBm jamming scenario. This omission is due to the receiver's severely compromised ability to track satellites in the GPS L1 band, with an average satellite visibility reduced to merely 1-2 satellites. In the absence of jamming, as shown in Fig. 4(a), the pseudorange residuals for all satellites remain consistently close to zero, within the range of -2 to 2 meters. In the presence of -105dBm (-10dB of JSR) and -97dBm (-2dB of JSR) jamming scenarios, most satellites still maintain residuals near zero, whose performance remains consistent with the no-jamming scenario. As the jamming power level increases, the pseudorange residuals exhibit increasingly fluctuations, particularly as that of the satellite (PRN=29) shown in Fig. 4(e). Additionally, obvious measurement outliers occur when the JSR exceeds 6dB. Due to the limitations of axis scales, several outliers reaching tens or even hundreds of meters in the 14dB and 22dB scenarios are not displayed in the figure, which also significantly threatens the reliability of the positioning solution. In Fig. 4(f), the receiver totally lose the tracking of PRN 29, and a noticeable instability in satellite tracking can be

**Table 1:** Parameters of GNSS, UWB and interference signals.

Type	Parameters	Descriptions
GNSS	Received power	About -95dBm
	Frequency band	1575.42 MHz / GPS L1
	Measurement Output Rate	5 Hz
	Scenario duration	GPST, 13:30 18/03/2024 to 15:00 18/03/2024
UWB	Output frequency	20 Hz
	Center frequency	3.9936 GHz
Interference	Center frequency	1575.42 MHz / GPS L1
	bandwidth	16 MHz
	Sweep period	25 $\mu s$
	Jamming powers	-105dBm, -97dBm, -89dBm, -81dBm, -73dBm, -65dBm
	JSRs	-10dB, -2dB, 6dB, 14dB, 22dB, 30dB
Duration of each scenario		6 min

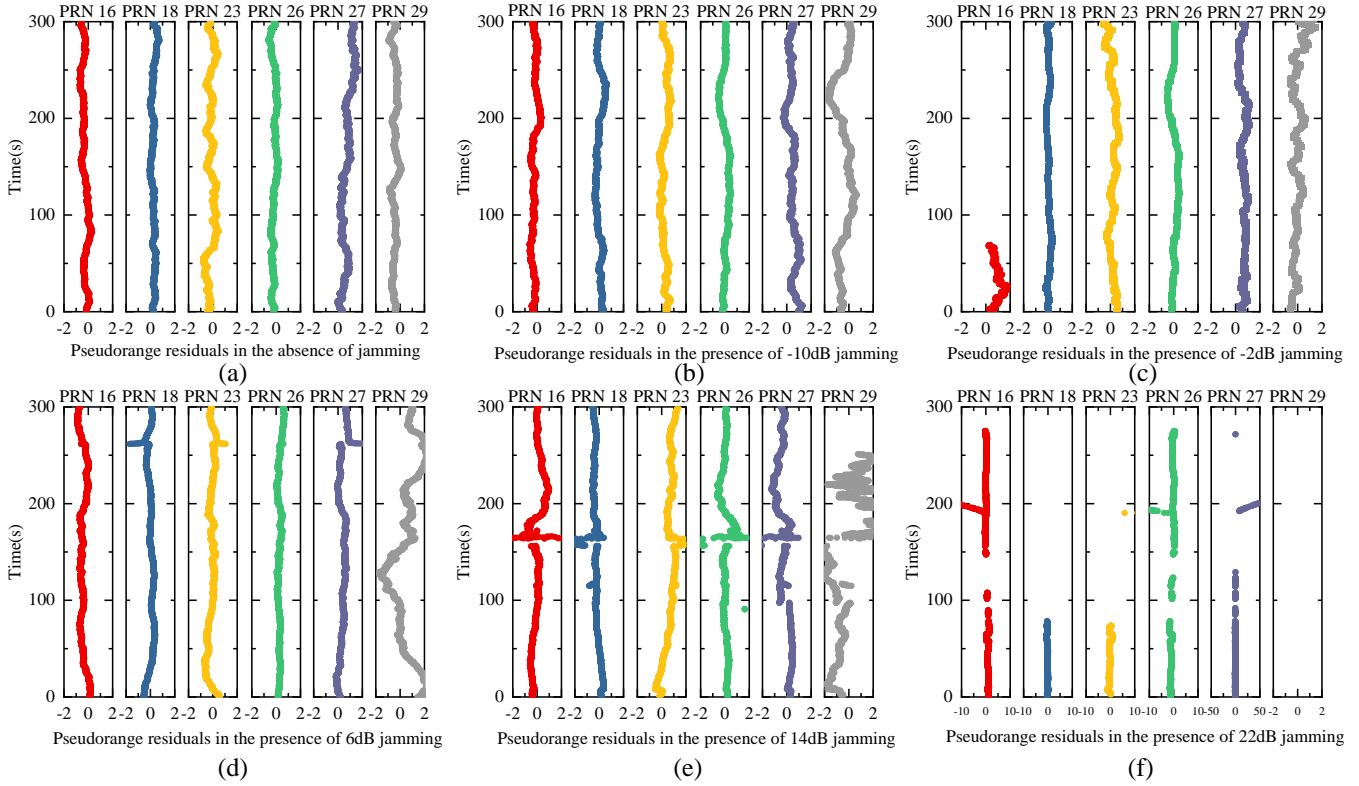


**Figure 4:** Pseudorange residuals from six satellites for various JSRs tested.

observed, indicating that the receiver has reached a critical threshold of tracking performance.

To evaluate the proposed UWB-enhanced TC integration method for jamming mitigation, the GNSS SPP and the dynamic positioning solution using filter (GNSS Filter) are compared with the proposed solution with respect to the horizontal errors. The horizontal errors for the three solutions are depicted in Fig. 5(a)-(f). The top three sub-figures (a-c) illustrate similar performance among the three solutions evaluated, maintaining tight clustering across a specific point. This emphasizes the receiver is minimally affected by the jamming signals at these levels, remaining the relative good performance. However, the proposed solution consistently achieves higher positioning precision, benefiting from the integration of UWB ranging measurements. The bottom three subfigures (d-f) in Fig. 5 exhibit degraded performance compared to the top three attributing

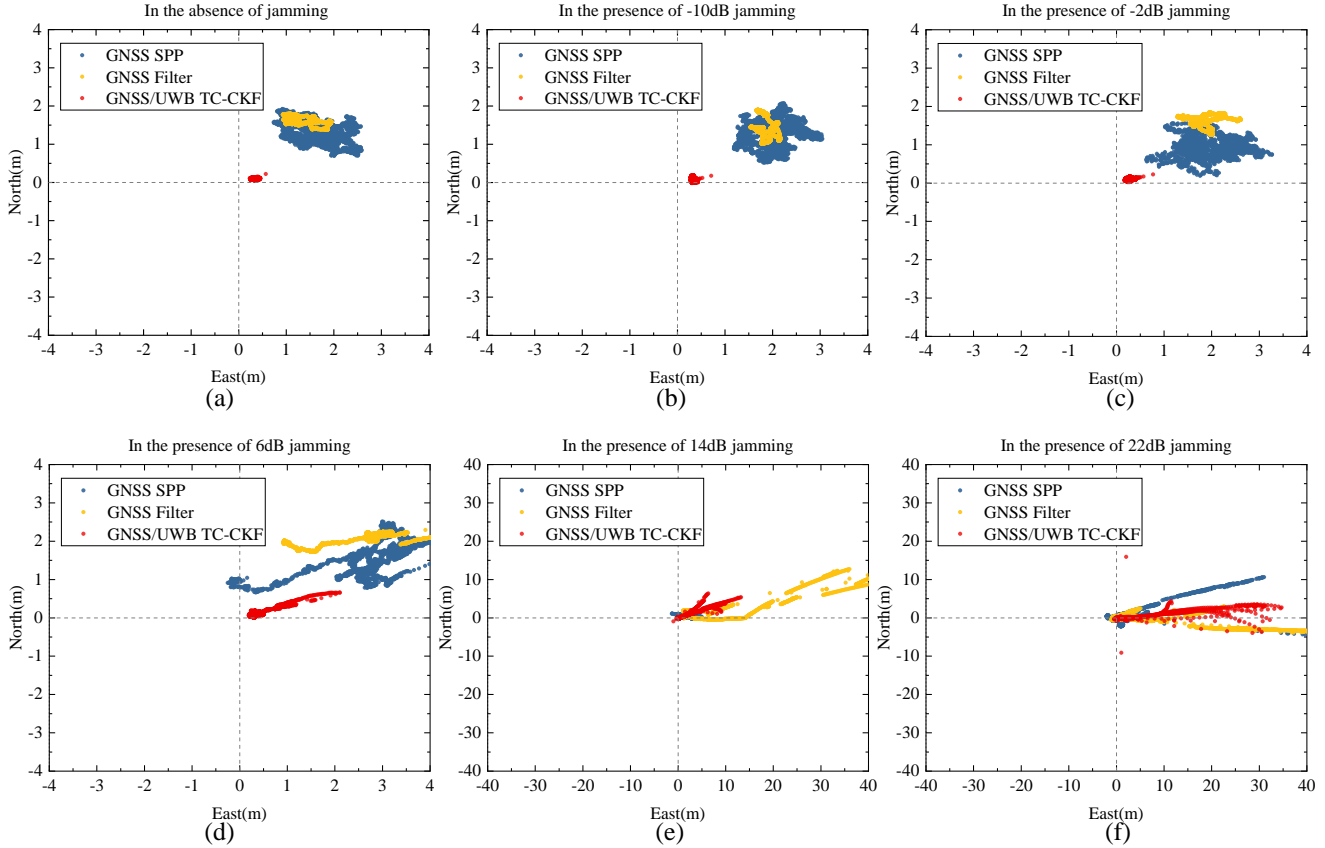


**Figure 5:** Horizontal errors for various JSRs tested.

to the higher jamming powers. There are also some severer outliers that far beyond the display range of the axis where most of the error points are located. This results in extreme positioning outliers for the SPP solution and partial convergence damage for the filter-based methods. These issues will be further displayed in the error over time plots below.

For further analysis of the impact of UWB ranging measurements on the positioning solution in the proposed solution, we display two typical scenarios in Fig. 6 and 7. The time-error results in the 14dB and 22dB scenarios are shown in the figures with respect to the positioning results and the velocity results. In Fig. 6, several positioning outliers can be observed from the GNSS SPP solution, while the GNSS Filter and the proposed solution shows a significant improvement of precision. Notably, after experiencing outliers, both the GNSS Filter and the proposed solution struggle to return to a normal level of positioning accuracy, indicating a challenge in fully recovering from severe outlier disruptions caused by jamming. This phenomenon can be attributed to a drawback of the Kalman filter family, where anomalous outliers can pollute the filter's parameters. Even in the presence of significant measurement errors caused by outliers, the measurement model continues to operate under the assumption of predefined noise levels. The Kalman filter, inherently reliant on Gaussian noise assumptions, struggles to adequately adjust to sudden, large outliers from the expected error distribution, thereby hampering its ability to accurately converge to true positioning after disruptions.

In both Fig. 6 and Fig. 7, there is no obvious improvement in the velocity errors of the proposed solution compared to the GNSS Filter solution. Due to the ranging nature that UWB measurements offer, only the positioning estimation can benefit from the additional UWB ranging measurements, instead of the velocity estimation. Consequently, in this test, while UWB can significantly reduce the positioning errors by providing accurate distance estimates, it does not contribute to the estimation of velocity significantly.

Additionally, for further demonstrate the effect of UWB measurements on the positioning results, we present the outcomes associated with varying numbers of UWB anchors used in our post-processing analysis in Fig. 8. Fig. 8 depicts the cumulative distribution of three-dimensional (3D) positioning errors across two scenarios, characterized by jamming-to-signal ratios (JSRs) of 14dB and 22dB. During the analysis, measurements with residuals exceeding 100m were identified as clear outliers that were

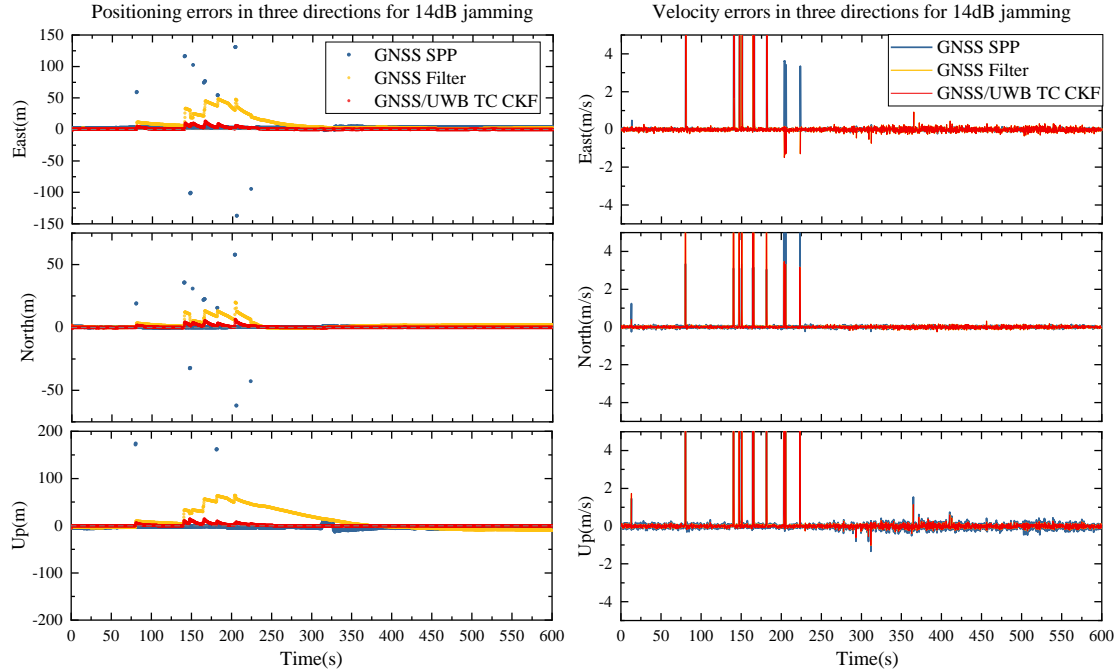


**Figure 6:** Positioning and velocity errors under 14dB jamming

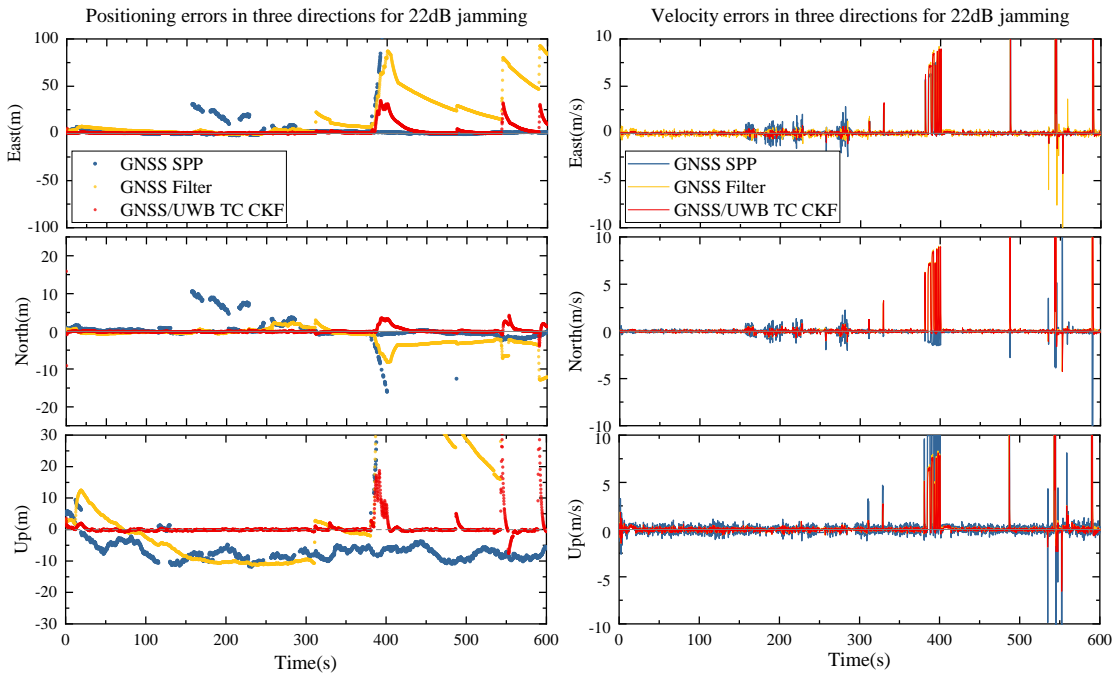


**Figure 7:** Positioning and velocity errors under 22dB jamming

excluded from the dataset fed into the processing procedure, which help us to clarify the influence of UWB measurements on the results. The filter-realized solution exhibits an improvement over SPP solution, when the outliers don't pollute the results, especially when with the UWB measurements. In the left subfigure, it is notable that when utilizing two Ultra-Wideband (UWB) anchors for positioning, there is a significant improvement in position accuracy compared to using only one anchor. In the right subfigure, Even with a single UWB anchor, there is a noticeable improvement over the GNSS SPP and Filter solution. The utilization of UWB technology, even with a limited number of anchors (two anchors, or even one anchor), contributes markedly

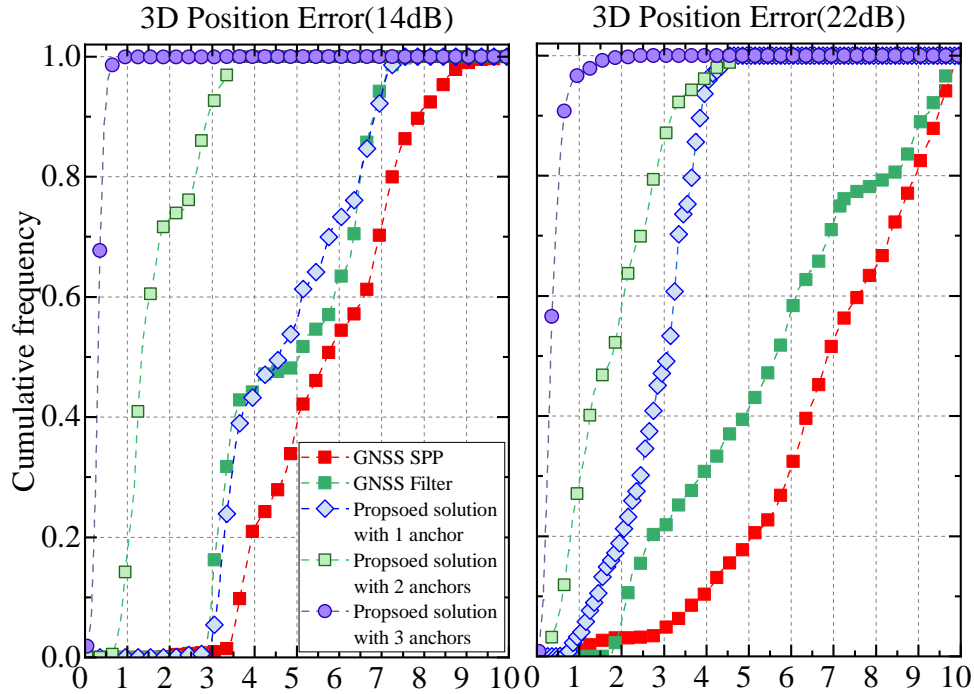


**Figure 8:** Cumulative distribution of three-dimensional (3D) positioning errors

to the reduction of errors associated with PVT estimation, demonstrating the effectiveness of UWB anchors in augmenting the resilience of positioning systems against interference signals.

## V. CONCLUSION

This research proposes a resilient positioning solution based on the UWB and GNSS to tolerate GNSS interference signals. Aiding with ranging measurements from UWB, a TC integration for GNSS and UWB using CKF is proposed in this research. We leverage UWB measurements to mitigate GNSS interference in the measurement domain, offering a cost-effective approach to interference effect suppression. This method enables the preservation of positional integrity without necessitating modifications to the receiver’s architecture, thereby preventing degradation or failure of positioning functions directly from the GNSS. To evaluate the proposed solution, a GNSS jamming test platform was developed, which combines open-sky GNSS signals with simulated interference. Subsequently, real-world UWB measurement collection was employed to conduct tests on the proposed solution under various levels of jamming powers. The results reveal that the proposed solution is capable of achieving an enhanced performance level over the GNSS SPP and Filter solutions.

Looking ahead, the challenge of convergence in the presence of significant outliers under jamming conditions remains. Future work will focus on enhancing this mitigation strategy to more effectively suppress the adverse effects of outlier pollution.

## ACKNOWLEDGEMENTS

This research was supported by National Natural Science Foundation of China (T2222015, U2268206, 62027809), Beijing Natural Science Foundation (4232031), and Technological R&D Program of China State Railway Group Co., Ltd. (K2023X002). The Ph.D. work of Zhuojian Cao and Yihan Guo in Politecnico di Torino is supported by the Chinese Scholarship Council (CSC) scholarship program. The Ph.D. work of I. Ebrahimi Mehr is supported by the grant DOT1332092 CUP E11B21006430005 funded within the Italian Programma Operativo Nazionale (PON) Ricerca e Innovazione 2014-2020, Asse IV “Istruzione e ricerca per il recupero” con riferimento all’Azione IV.4 “Dottorati e contratti di ricerca su tematiche dell’innovazione” e all’Azione IV.5 “Dottorati su tematiche green” DM 1061/2021.

## REFERENCES

- Abbasi, M., Mosavi, M. R., and Rezaei, M. J. (2020). GPS continues wave jamming canceller using an ANF combined with an artificial neural network. In *2020 8th Iranian Joint Congress on Fuzzy and Intelligent Systems (CFIS)*, pages 099–104. IEEE.
- Abd El Rahman, M., Elharmel, M., Abdelrasol, R., Zaghloul, M., and Elghamry, M. (2021). GNSS interference suppression techniques: A survey. *International Journal of Telecommunications*, 1(01):1–10.
- Aiello, G. R. and Rogerson, G. D. (2003). Ultra-wideband wireless systems. *IEEE microwave magazine*, 4(2):36–47.
- Arasaratnam, I. and Haykin, S. (2009). Cubature kalman filters. *IEEE Transactions on automatic control*, 54(6):1254–1269.
- Borio, D., Dovis, F., Kuusniemi, H., and Presti, L. L. (2016). Impact and detection of GNSS jammers on consumer grade satellite navigation receivers. *Proceedings of the IEEE*, 104(6):1233–1245.
- Cao, Z., Liu, J., Jiang, W., Cai, B., and Wang, J. (2022). INS/Odometer/Trackmap-aided railway train localization under GNSS jamming conditions. In *2022 IEEE Intelligent Vehicles Symposium (IV)*, pages 427–434. IEEE.
- Commission, F. C. et al. (2002). Revision of part 15 of the commission’s rules regarding ultra-wideband transmission systems. *First Report and Order FCC 02-48*.
- DecaWave (2015). DW1000 datasheet.
- Ding, M., Chen, W., and Ding, W. (2023). Performance analysis of a normal GNSS receiver model under different types of jamming signals. *Measurement*, 214:112786.
- House, W. (2013). Presidential policy directive (PPD) 21. *Critical Infrastructure Security and Resilience (Washington, DC: White House)*.
- Kaplan, E. D. and Hegarty, C. (2017). *Understanding GPS/GNSS: principles and applications*. Artech house.
- Kraus, T., Bauernfeind, R., and Eissfeller, B. (2011). Survey of in-car jammers-analysis and modeling of the RF signals and IF samples (suitable for active signal cancelation). In *Proceedings of the 24th International Technical Meeting of The Satellite Division of the Institute of Navigation (ION GNSS 2011)*, pages 430–435.
- Medina, D., Lass, C., Marcos, E. P., Ziebold, R., Closas, P., and García, J. (2019). On GNSS jamming threat from the maritime navigation perspective. In *2019 22th International Conference on Information Fusion (FUSION)*, pages 1–7. IEEE.
- Morales Ferre, R., de la Fuente, A., and Lohan, E. S. (2019). Jammer classification in GNSS bands via machine learning algorithms. *Sensors*, 19(22):4841.
- Singh, A. K. (2020). Major development under gaussian filtering since unscented Kalman filter. *IEEE/CAA Journal of Automatica Sinica*, 7(5):1308–1325.
- Yinusa, K. A., Marcos, E. P., and Caizzone, S. (2018). Robust satellite navigation by means of a spherical cap conformal antenna array. In *2018 18th International Symposium on Antenna Technology and Applied Electromagnetics (ANTEM)*, pages 1–2. IEEE.
- Zhang, J., Cui, X., Xu, H., and Lu, M. (2019). A two-stage interference suppression scheme based on antenna array for GNSS jamming and spoofing. *Sensors*, 19(18):3870.
- Zhong, W., Xiong, H., Hua, Y., Shah, D. H., Liao, Z., and Xu, Y. (2024). TSFANet: Temporal-spatial feature aggregation network for GNSS jamming recognition. *IEEE Transactions on Instrumentation and Measurement*.